Aero-Spaceplane Mission Performance Estimations Incorporating Atmospheric Control Limits

Jack A. Griffin[1]
and
Timothy T. Takahashi[2]

Arizona State University, Tempe, AZ, 85281, US

This paper describes the extension of an aircraft-style time-step integrating mission performance simulation to address the aero-spaceplane design challenge. Aircraft style flight at very high speeds and altitudes requires enhancements to the typical point-mass simulation including: 1) implementing an atmosphere model valid to near-space conditions, 2) considering large-angle (rather than small-angle approximate) equations of motion, 3) including centripetal accelerations from forward flight which oppose gravity, 4) permitting ballistic and quasi-ballistic flight at atypical load-factors by offering constant-alpha or constant-C_L flight modes, 5) enabling flight at high-bank angles to mitigate tendencies for "atmospheric skip," 6) tracking the Short-Period and Dutch-Roll rigid-body modes to understand time-domain limits to aerodynamic control and 7) monitoring the Lateral Control Departure Parameter (*LCDP*) to ensure that the aircraft is not spin prone. We showcase our revised algorithm by re-creating some of the missions flown by the famous North American X-15 rocket plane including its "astronaut wings" flights. We closely match the kinematics of several flight trajectories and predict the strong inherent stability and innate controllability of the X-15 as observed in flight test.

Nomenclature

alt	= altitude, ft
α	= angle-of-attack, deg (°) or radians
b	= span, ft
β	= side-slip-angle, deg (°)
$\bar{c}$	= mean geometric chord, ft
C_L	= coefficient of lift
C_D	= coefficient of drag
$dC_l/dAILERON$	= rolling moment due to aileron defl
$dC_l/d\beta$	= rolling moment due to side slip
$dC_m/d\alpha$	= pitch stability
$dC_n/dAILERON$	= yaw moment due to aileron defl
$dC_n/d\beta$	= yaw moment due to side slip
dELEV	= elevator deflection, deg
Ixx	= rolling moment of inertia, slug-ft^2
Iyy	= pitching moment of inertia, slug-ft^2
Izz	= yawing moment of inertia, slug-ft^2
KEAS	= knots equivalent airspeed
KTAS	= knots true airspeed
M	= Mach number
MTOW	= maximum takeoff weight, lbm
n, nZ	= load factor,-gees
q	= dynamic pressure, lbf/ft^2
S_{ref}	= reference area, ft^2
t	= time, sec
TTD_{sp}	= Short-Period time-to-double, sec
TTD_{dr}	= Dutch-Roll time-to-double, sec
W	= weight, lbm
ω_{sp}	= Short-Period freq, Hz or rad/sec
ω_{dr}	= Dutch-Roll freq, Hz or rad/sec
φ	= bank angle, deg (°)
ρ	= air density, slug/ft^3

[1] M.S. Candidate, Aerospace Engineering, Ira A. Fulton Schools of Engineering, Arizona State University, Tempe, AZ, 85287.
[2] Professor of Practice – Aerospace Engineering, School for the Engineering of Matter, Transport and Energy, Arizona State University, Tempe, AZ, 85287. AIAA Associate Fellow.

I. Introduction

HYPERSONIC vehicles and Aero-Space planes made newsworthy flights in 2021. On July 11, Virgin Galactic successfully flew their rocket plane to the edge of space [1]. In July, Russia announced test flights of its newly developed "Zircon" hypersonic air-breathing "cruise-missile" demonstrator [2]. In September, the United States Air Force announced a successful flight of a Raytheon developed air-breathing hypersonic missile demonstrator [3]. Such flight vehicles combine elements of conventional aircraft as well as launch vehicles.

Aircraft performance simulations typically define the flight path by a sequence of commands intelligible to a pilot. Pilots typically fly aircraft at constant indicated airspeed, constant Mach Number or constant altitude. [4][5][6] The engines may run at a prescribed power setting (such as military power or flight-idle) or throttled back to maintain flight at constant speed and altitude where thrust is in equipoise with drag. While explicit simulations define key trajectory shaping elements such as target altitudes, speeds and distances, other important state variables such as flight path angle or angle-of-attack become implicit byproducts. For example, if thrust exceeds drag, the aircraft can either accelerate or climb. If thrust equals drag, the aircraft will "fly" in steady and level. If thrust is less than drag, the aircraft can decelerate or descend. Whether the aircraft is above or below its target speed or altitude controls whether or not excess thrust is used to accelerate and/or climb. These simulations derive a speed / altitude profile directly from the state variables (speed, altitude and/or angle-of-attack) used to control its flight.

In contrast, launch-vehicle performance simulations traditionally define the flight path by a series of commands that are directly intelligible to a GN&C system. Implicit simulation methods have been used to define trajectories for missiles as well as launch vehicles. POST and OTIS are popular programs that formulate and optimize spacecraft ascent trajectories. OTIS is an acronym for *Optimized Trajectory by Implicit Simulation*. [7] POST is an acronym for *Program to Optimize Simulated Trajectories*. [8] Launch-vehicle codes define a trajectory by developing a time-history of attitudes (angle-of-attack (α) and side-slip-angle (β)) and throttle position. While such a trajectory is entirely reasonable from a control-theory perspective, and perhaps the most suitable means to support launch-vehicle or air-to-air missile design, these codes only **implicitly** control speed and altitude.

Unlike pilot-centric explicit simulations, implicit, GN&C based trajectory design does not directly account for the aerodynamics of the vehicle. GN&C simulations, by their choice of state variables, must omit many lessons-learned and common-practices developed from over 100 years of wing-borne piloted flight. In a conventional launch vehicle scenario, this distinction is moot because there is little lift generated by the vehicle. When developing high performance winged vehicles, the choice of implicit simulation state-variables might cloud insights that could otherwise be exploited when developing novel high-performance aircraft.

We are not the first authors to seriously consider the use of a traditional aircraft performance approach to architect hypersonic vehicle trajectories. In 1991, Kauffman, et al utilized classic energy maneuverability methods to devise an efficient rocket / turbine based combined cycle ascent profile [9]. Their work noted that concurrent rocket / air-breathing system operation, as opposed to sequential air-breathing / rocket operation, could improve the vehicle payload fraction to orbit [9]. Kauffman later noted that theoretically "optimal" trajectories could easily excite Phugoid motions as the vehicle attempts to follow a prescribed speed / altitude schedule; for example, a transition from a climb at constant dynamic pressure to a climb at constant Mach Number [10]. This work did not directly consider other longitudinal or lateral-directional handling qualities metrics when shaping trajectories.

The North American X-15 rocket plane is an excellent example of a hypersonic winged aircraft, flown by pilots according to aircraft-style flight procedures [11]. In this paper, we use it as a benchmark to extend an aircraft-style time-step integrating mission performance simulation to be able to address the challenges inherent in aero-spaceplane design.

FIGURE 1 – X-15 Pilots Flight Manual [11]

Aircraft style flight at very high speeds and altitudes requires enhancements to the typical point-mass simulation. In this paper, we will describe how we move beyond the FAA 1962 Standard Atmosphere to implement the full 1976 standard atmosphere model; this is valid from sea-level to near-space conditions [12]. We will also describe the need to incorporate large-angle (rather than small-angle approximate) equations of motion, use the geo-potential gravity model to address flight at very high altitude and also include the centripetal acceleration terms arising from forward flight which oppose gravity. We will describe how we can define ballistic and quasi-ballistic flight at atypical load-factors; we implement "constant α" and "constant C_L" flight modes to provide a broader selection of flight styles than that attainable with the typical "level flight" or "climb at constant airspeed" functionality of an airplane style simulation.

While aircraft style point-mass models typically allow flight at $nZ \neq 1$, we also realized that the X-15 in order to mitigate tendencies for "atmospheric skip" flew portions of re-entry at $nZ >> 1$ and at high bank-angles. This strategy requiring high alpha flight at $nZ >> 1$ for aerodynamic braking while banking over at a severe angle ($\varphi > 45°$) enabled the vehicle to decelerate during descent. The fact that the X-15 turns during this maneuver is a byproduct of the need for aerodynamic braking; this is opposite to a typical aircraft – which only inadvertently loses altitude due to a need to change heading.

The X-15 flew both high-speed endo-atmospheric and exo-atmospheric flights. [13][14][15] Many X-15 trajectories took the aircraft to such altitudes that despite its hypersonic speed, dynamic pressure dropped far below its "1-gee stall speed." As the pilots earned their "astronauts wings" they flew the X-15 "over-the-top" of a nearly ballistic trajectory that had aerodynamic control diminish to the point of needing to supersede conventional control strategies with bursts of reaction control jets. [13] Since the X-15 was intrinsically aerodynamically stable at all speeds and flight attitudes, the need for reaction control jets comes from the time-domain problem. [13] On ascent, as the aircraft progressively flies into a more rarefied atmosphere, the aerodynamically driven rigid-body modes (the Short-Period and Dutch-Roll) diminish to such low frequencies that it becomes impossible to use aerodynamic control with reasonable phase margin to follow the required trajectory. Conversely, on descent, if the aircraft flew in a denser atmosphere at hypersonic speeds, the aerodynamically driven rigid-body modes (the Short-Period and Dutch-Roll) could rise to such a high frequency that they would overlap structural resonances and cause the aircraft to "shake itself to pieces."

In the following sections, we will describe in detail how we enhanced an aircraft-style point-mass mission simulation to be able to successfully model a variety of X-15 flights. This code is a time-step marching simulation that solves the basic point-mass equations of motion based on flight weight, aircraft speed and altitude and aircraft attitude (where the angle-of-attack can be either specified for quasi-ballistic flight or implied to maintain constant speed and/or altitude). To enhance the usability of the code to assess stability and controllability issues, at each time step the code computes a variety of screening parameters necessary to identify if the point-mass model has the aircraft operate in a manner which exceeds its longitudinal trim capability, excites inertial coupling or exposes it to control coupling. The code also estimates the stick fixed Short-Period and Dutch-Roll mode frequency which helps identify regions of the trajectory that may need reaction-control system augmentation.

This "intermediate fidelity" analysis is useful to help screen candidate designs. Unlike a full 6-DOF simulation, the engineer need not develop control laws prior to running this code. At the same time, this code is "agnostic" to the source of its input data: the aerodynamic database may be developed from semi-empirical methods, panel method codes, CFD, wind-tunnel or even flight test basis. Similarly, the propulsion "five-column data" may derive from a variety of models. Thus, this tool is flexible to support conceptual, preliminary and detail design.

II. Populating and Post Processing the Aerodynamic and Mass Properties Database

In order to "fly" a simple mission we need a basic aero database. The contents of this database consist of functions in terms of three independent variables. First, there is the weight of the X-15 which varies between its launch weight and its fuel exhausted conditions. Then there is the Mach Number which varies from the low subsonic (approach and landing), to the record braking Mach 6+. Last, there is the angle-of-attack which has measures from 0^o to 20^o; allowing for the high angle-of-attack operations flown during speed bleeding aero-braking maneuvers returning from exo-atmospheric flights. Since the simulation is constantly determining its own conditions, it can perform a trilinear interpolation at flight conditions to pull the desired dependent variables. The dependent variables are trimmed lift

coefficient C_L(M, α), drag coefficient C_D(M, α), center of gravity location *XCG*(W), moments of inertia *Ixx*(W), *Iyy*(W), *Izz*(W), elevator deflection *dELEV*(M, α), and stability parameters of $dC_m/d\alpha$(M,α), *Cnβdynamic*(W,M,α), and *LCDP*(W,M,α).

A. Developing the Longitudinal Aerodynamic Database

Our main aerodynamic database derives from a cocktail approach using a Vortex Lattice model [16] of the X-15 in the small ventral tail configuration; see FIGURE 2. While the X-15 was originally conceived to have a symmetrical dorsal and ventral fin, most high-speed X-15 flights were flown with much of the ventral fin removed. The vast majority of wind tunnel data collected represented the initial configuration with the large ventral. [17][18][19] [20][21][22][23][24] Available X-15 wind tunnel data derives from a variety of sources including the NASA/Langley Unitary Plan Wind Tunnel, [20][23] and the NASA/Langley 11-inch hypersonic blowdown tunnel [23][24] among others. Because only a fraction of the total wind tunnel data set modelled the final flight configuration, we began with our Vortex Lattice model of the small ventral flight configuration and "adjusted" the data where necessary (zero-lift drag and wedge-tail-deployed directional stability) to better represent the flight test configuration.

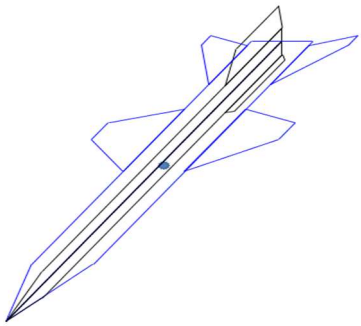

FIGURE 2 – VORLAX model of the X-15

VORLAX is a vortex lattice potential flow solving CFD code written in FORTRAN [16] and recently received updates that drastically improve performance. [25] VORLAX is especially useful for determining stability derivatives. VORLAX develops influence coefficients for both subsonic and supersonic leading edge flow. We note that its supersonic model only accounts for shock waves developed at the leading and/or trailing edges; as such it is valid for "slender" shapes that do not develop off-body standing shock waves. In addition, VORLAX solutions fundamentally neglect thickness effects, and as such will under-predict the directional stabilizing effect of the X-15 wedge tail. It also cannot capture any sort of "real-gas-effects" of high temperature air. Despite these limitations, we demonstrate here how well it captures the essential aerodynamic properties of the X-15 from subsonic through the hypersonic.

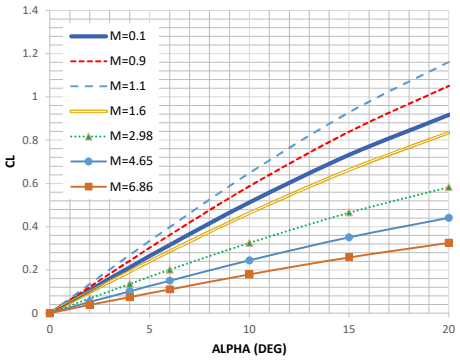

FIGURE 3 – C_L vs α from VORLAX "cocktail" aero database

VORLAX inputs a detailed geometry via a collection of panels to represent the aircraft airframe and control surfaces; see FIGURE 2. In addition to angle-of-attack, Mach Number, sideslip, and control surfaces deflections. The results are exported in an easily parsed text format.

Table 1 Buffet CL

Mach	CLmax
0.1	0.488
0.6	0.411
0.9	0.360

We built our X-15 aerodynamic database around our VORLAX model. FIGURE 3 plots VORLAX derived estimates of "trimmed" C_L vs α. We note that there are trust-zone limits $C_L max$(M) for flight at $M < 1$ where C_L is stall or buffet limited. This is derived from an EDET [26] model of the X-15 and shown in Table 1. For flight at $M>1$, the usable aerodynamic database is limited solely by angle-of-attack ($0<\alpha<20^o$). We found that the VORLAX model lift-slope closely agreed with Saltzman & Garringer; FIGURE 4. [27]

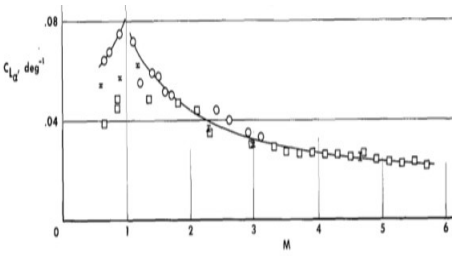

FIGURE 4 – $dC_L/d\alpha$ as a function of Mach Number from NASA TN D-3343 [27]

The *CD* values start from the Vortex Lattice model. However, as it is an inviscid solver a zero-lift drag correction is needed. Altitude dependent Reynolds Number corrections, $\Delta CD(M,ALT)$, also derived from an EDET model of the X-15. [26] Basic zero-lift-drag corrections derive from X-15 flight test results as collated by Saltzman & Garringer [27] and Saltzman [28]; see Table 2 and FIGURE 5. The "cocktail" database results are shown in FIGURE 6.

Table 2: Vortex Lattice Zero-Lift Drag Correction

M	C_{D0}
0.1	0.0540
0.7	0.0600
0.9	0.0700
1.1	0.1300
1.6	0.0900
1.9	0.0800
2.29	0.0700
2.98	0.0600
4.65	0.0450
6.86	0.0350

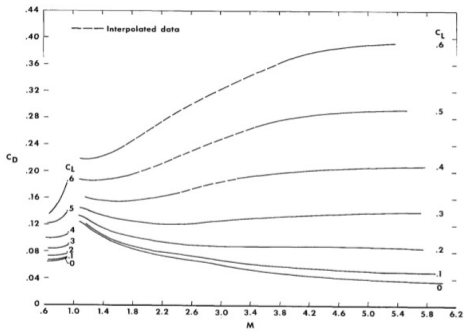

FIGURE 5 – $C_D(C_L, M)$ from NASA TN D-3343 [27]

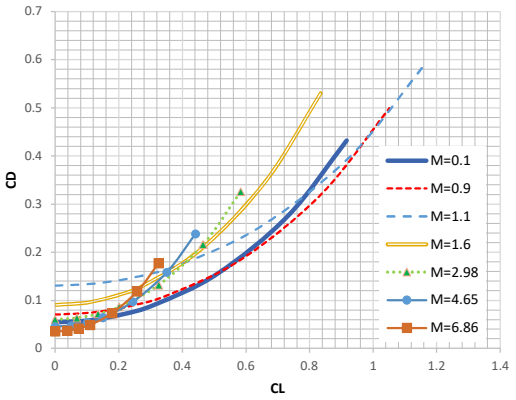

FIGURE 6 – C_D vs α from VORLAX "cocktail" aero database (VORLAX with zero-lift-drag offset to match Flight Test data)

B. Post Processing the Longitudinal Aerodynamic Database

On very high speed aircraft, pressure coefficient limits due to vacuum radically limit leeward side pressures at hypersonic speeds. As a result, vehicle aerodynamics becomes dominated by windward side geometry. While we expect aircraft to demonstrate changes in aerodynamic center position as a function of Mach Number, hypersonic aircraft at high-speeds have marked shifts in aerodynamic center-position as a function of Mach Number, lift coefficient and pitch-control surface deflection angle. Some hypersonic aircraft might even trim at two different C_Ls with the same elevator setting. Thus, to make reasonable estimates on controllability in pitch, the aerodynamic database should contain the pitch-trim aerodynamic surface deflection needed to trim and $dC_m/d\alpha$ as both a functions of flight weight, CG position, Mach and angle-of-attack. We need to track both the deflection to trim and $dC_m/d\alpha$ as high-speed vehicles are likely to have extremely high fuel fractions with concomitant changes in CG position that along with significantly non-linear aerodynamic characteristics impact control power and longitudinal stability.

To determine if the aircraft is capable of being trimmed in pitch throughout the flight, we calculate the required elevator with the intention that if the aircraft requires an unrealistic elevator deflection, then the aircraft clearly cannot be trimmed for that angle-of-attack. As the required deflection is not something we want to determine during the simulation it is included in the extended aero performance data. Where at each Mach Number and angle-of-attack, VORLAX is used to calculate the pitching moment at zero and 30° deflections. Then by simply linearly interpolating the required deflection to achieve trim, as shown in Equation 1 below. We then can arrive at the required elevator to trim, see Table 3. With the table agreeing with FIGURE 7; overleaf.

$$dELEV = 30° * \left(\frac{Cm(ELEV=0°,\alpha)}{Cm(ELEV=30°,\alpha) - Cm(ELEV \quad °,\alpha)}\right) \tag{1}$$

Table 3 Elevator to Time from "cocktail" aero database

Alpha	M=0.1	M=0.7	M=0.9	M=1.1	M=1.6	M=2.26	M=2.98	M=4.65	M=6.86
20	10	9.6	8.4	6	38.1	35.9	30.3	29.8	32.7
15	7.6	7.3	6.4	4.5	29.3	27.4	23.2	23	25.3
10	5.1	4.9	4.3	3.1	20.1	18.8	15.8	15.9	17.5
6	3.1	3	2.6	1.9	12.4	11.5	9.7	9.9	10.8
4	2.1	2	1.8	1.2	8.4	7.8	6.6	6.7	7.4
2	1.1	1	0.9	0.6	4.2	4	3.3	3.4	3.7
0	0	0	0	0	0	0	0	0	0

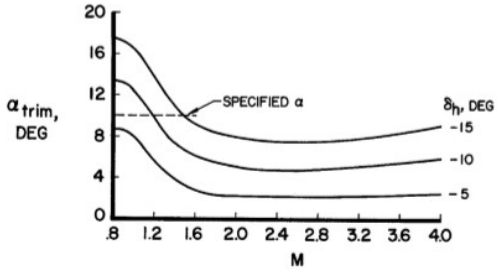

FIGURE 7 – Elevator to Trim from NASA TM X-715 [19]

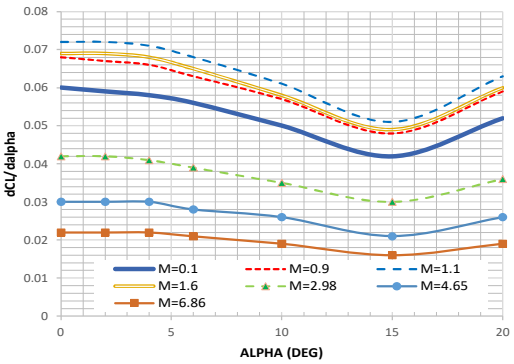

FIGURE 8 – $dC_L/d\alpha$ vs α from VORLAX "cocktail" aero database

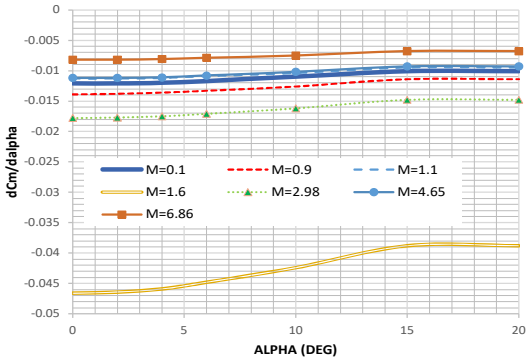

FIGURE 9 – $dC_m/d\alpha$ vs α from VORLAX "cocktail" aero database

As a stable aircraft flies, it will exhibit a natural "bobbing" motion in both a pitching (the "Short-Period") and in a coupled rolling-and-yawing mode (the "Dutch-Roll"). For an aircraft to be aerodynamically controllable we must have an agreeable short-period frequency. Too fast, and the airplane's rigid body mode excites structural resonance. Too slow, and the pilot finds the controls to be "mushy" with substantial phase-lag that provokes pilot-induced oscillations.

To estimate the dynamic, rigid-body modes associated with flight, we need to document the pitch responsiveness ($dC_L/d\alpha$) and longitudinal stability ($dC_m/d\alpha$). In each case, we numerically differentiate data found in our basic aerodynamic database. We show these derivatives as functions of Mach Number and angle-of-attack in FIGURES 8 and 9.

To predict the longitudinal "Short-Period" frequency, we use a one-degree-of-freedom dynamic model. The aircraft is represented as a pair of lumped masses (defining the mass-moment-of-inertia) and a torsional spring derived from the aerodynamic stability in pitch, $dC_m/d\alpha$; see FIGURE 10. If the system is stable, then there will be some frequency at which it oscillates at, but in the case in which the system is unstable we would like to understand how quickly the system will diverge, a common metric calculated is the time-to-double.

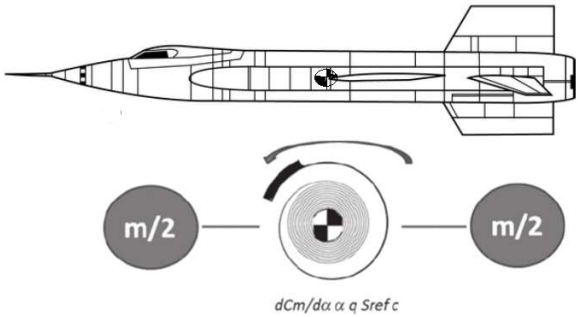

FIGURE 10 – Simplified one-degree of freedom short-period frequency model.

Frequencies for satisfactory flight are outlined in MIL-STD 8785C; see FIGURE 11. [29] The upper bound of the rigid-body "Short-Period" mode is one where the frequency is below that of primary structural resonance; typically, this will be a single digit frequency in Hz (i.e. 3-Hz) as predicted by structural finite-element-analysis. It is possible for this condition to develop when a very stable aircraft flies at extremely high dynamic pressure (*KEAS* >> 1000).

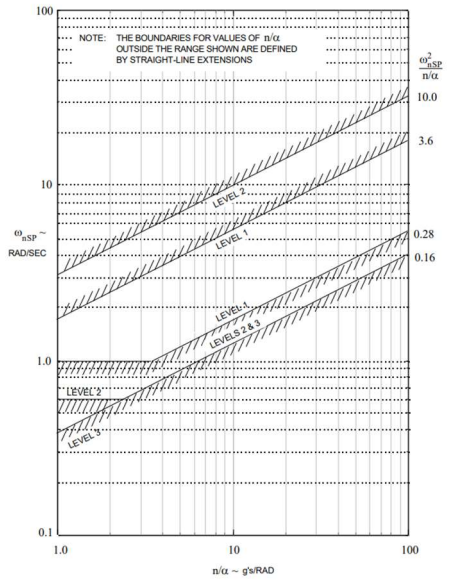

FIGURE 11 – Short-Period frequency requirements from MIL 8785-C "Category A" Flight Phases. [29]

MIL-STD 8785C defines aircraft into several classes based on their size and intended purposes: there are three categories of nonterminal flight of which we focus primarily on Category A. Category A flight implies active maneuvering whereas Category B is defined as "Climb" "Cruise" and "Loiter" (less demanding piloting conditions) or Category C which is defined for takeoff and landing (and is even more demanding to pilot). The primary X-15 flight falls under the Category A condition; refer back FIGURE 11.

MIL-STD 8785C defines three levels of "handling qualities" representing pilot workload as defined by the Short-Period frequency and pitch responsiveness of the airframe: *LEVEL 1* where the qualities are clearly adequate, *LEVEL 2* where flying qualities are adequate but requires a higher workload, and *LEVEL 3* where the aircraft is still safe but requires excessive workload.

From these specifications we will be able to analyze the characteristics of a high-speed aircraft, like the X-15 as it flies its mission.

MIL-STD 8785C (refer back to FIGURE 11) stipulates *LEVEL 1* qualities if the longitudinal parameter $\omega^2_{sp}/(n/\alpha)$ falls in the range $0.28 < \omega^2_{sp}/(n/\alpha) < 3.6$; with a floor of $\omega_{sp} = 1$ radian/sec (0.16 Hz or a 6.28 second Short-Period mode). *LEVEL 2* qualities if $0.16 < \omega^2_{sp}/(n/\alpha) < 3.6$; with a floor of $\omega_{sp} = 0.6$ radian/sec (0.095-Hz or a 10.5-sec Short-Period mode). *LEVEL 3* qualities exist so long as $\omega^2_{sp}/(n/\alpha) > 0.16$. If $\omega^2_{sp}/(n/\alpha) < 0.16$ the standard deems the aircraft unacceptably unresponsive.

Because the previously stated stability parameters depend on flight conditions, weight and moments of inertia, we must calculate them in the context of a proposed flight trajectory. Since flight conditions are continuously tracked by the point-mass kinematics of the mission code, we know the Mach Number, angle-of-attack (α), dynamic pressure and flight weight at each time step. From there, we can estimate pitch responsiveness at each time step along the trajectory as:

$$\frac{n}{\alpha} \approx \frac{57.4 \frac{dCL}{d\alpha} q\ Sref}{W} \tag{2}$$

In order to estimate the Short-Period frequency at each time step along the trajectory, we will need to estimate the mass-moment-of-inertia in pitch (*Iyy*) as a function of flight weight; we currently use simple linear interpolation. From there, we can estimate the Short-Period Frequency in Hz as:

$$\omega_{sp} \approx \left(\frac{1}{2\pi}\right) \sqrt{\frac{-57.4 \cdot dC_m/d\alpha \cdot q \cdot S_{ref} \cdot \bar{c}}{I_{yy}}} \tag{3}$$

The X-15, along with many Hypersonic Boost-Glide concepts, flew at extremely high altitudes. Despite the high Mach Number, the vehicle may actually fly a substantial portion of its mission at low dynamic pressure. Thus, we must consider the lower bounds of longitudinal responsiveness. To do so, refer once again to the MIL 8785C chart (FIGURE 11). As the aircraft leaves the atmosphere and *q* heads towards zero, *n/α* also heads towards zero. Note that if *n/α* ~

1.0-gee/radian (the lower bound of the chart) this metric implies trimmed flight at 1-gee (i.e. $nZ = 1$) to require 57.4 º angle-of-attack. So, the practical limit to trimmed (rather than quasi-ballistic flight) exists so long as $n/\alpha > 3$ (i.e. when 1-gee trimmed flight can exist at less than ~20º angle-of-attack).

For quasi-ballistic flight, where the aircraft may operate at or below $n/\alpha \sim 3$, we see that the minimum permissible *LEVEL 3* Short-Period frequency is ~0.4 radian/sec (0.06-Hz or a 15-second period). When the rigid body frequencies drop below that, the aircraft becomes hopelessly unresponsive to pilot using a conventional control strategy. If our mission code indicates such slow rigid body modes as the aircraft leaves the atmosphere, the GN&C system will need to abandon an aerodynamic control approach and revert to reaction-control jets.

In the case that the aircraft is statically unstable in pitch, $dC_m/d\alpha >= 0$. The useful metric is the stick-fixed time-to-double. That is found from the one-degree-of-freedom approximation with the following equation.

$$TTD_{sp} \approx \sqrt{\frac{I_{yy}}{57.4 \cdot dC_m/d\alpha \cdot q \cdot S_{ref} \cdot \bar{c}}} \tag{4}$$

MIL 8785C implies that it is impermissible to have a pilot operate an aircraft with unstable pitch characteristics displayed at the control stick. While the stick-fixed open-loop control of a statically unstable aircraft will exhibit a time-to-double, a feedback controller will synthesize $dC_m/d\alpha < 0$. The problem remains in that with finite control power, even a synthetic $dC_m/d\alpha$ cannot produce reasonable Short-Period frequencies as $q \rightarrow 0$.

C. Building the Lateral-Directional Aerodynamic Database

We next turn to the lateral-directional stability and controllability of the airframe. First, we will assess the stick-fixed lateral-directional stability as it pertains to the Dutch-Roll rigid body mode. Secondly, we will assess if the aerodynamic roll-control strategy implied by the control surface disposition unintentionally makes the aircraft prone to spin.

The basic stick-fixed lateral-directional stability as predicted by VORLAX may be seen below. A comparison of FIGURES 12, 13 and 14 shows that the VORLAX derived values follows the trend shown in NASA-TM-X-726 [32]. The "lower-rudder-off" configuration has weakly positive directional stability ($dC_n/d\beta > 0$) with rising stability up to $M = 1.6$. Above this speed, the X-15 deploys its wedge "speed brake" to enhance directional stability; see FIGURE 15. In our "cocktail database" we supersede the VORLAX data with $dC_n/d\beta \sim +0.008$; see FIGURE 15). In addition, the VORLAX model shows that the "lower-rudder-off" configuration has positive dihedral effect ($dC_l/d\beta < 0$) at all Mach Numbers. VORLAX captures an increase in effective dihedral around $M = 1.6$ shown in the "lower rudder on" wind tunnel data but neglected from the "estimated" lower rudder off" data.

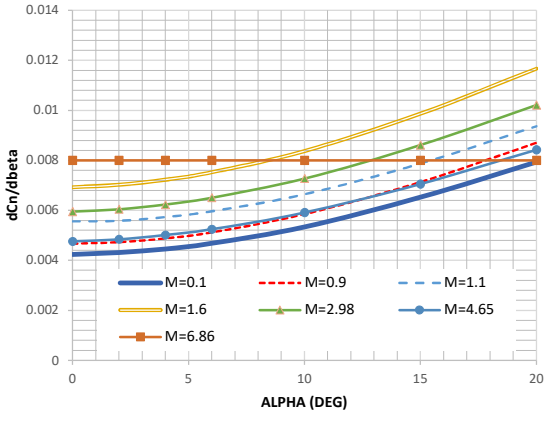

FIGURE 12 – $dC_n/d\beta$ vs alpha from VORLAX "cocktail" aero database

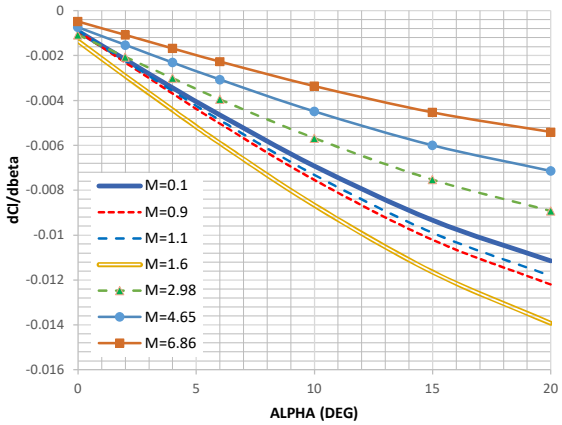

FIGURE 13 – $dC_l/d\beta$ vs alpha from VORLAX "cocktail" aero database

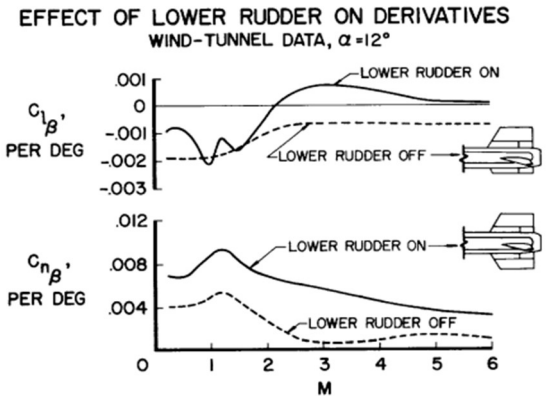

FIGURE 14 – Lateral-Directional Stability with Lower Rudder Off (the actual high-speed flight Configuration) from NASA [31]

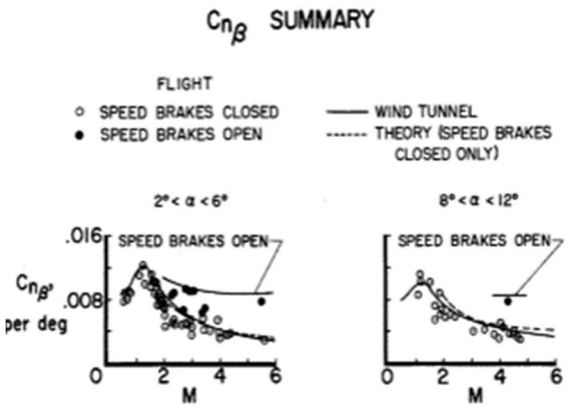

FIGURE 15 – Speed brake effect on directional stability from NASA X-714 [18]

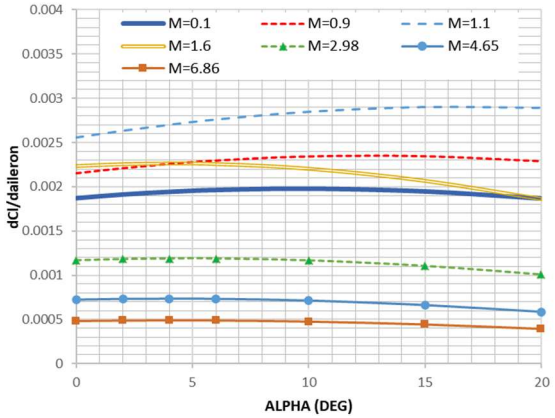

FIGURE 16 – *dCl/dAILERON* from differential elevon from VORLAX "cocktail" aero database

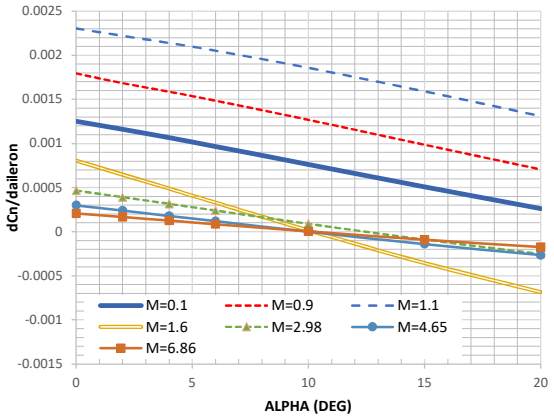

FIGURE 17 – *dCn/dAILERON* from differential elevon from VORLAX "cocktail" aero database

FIGURES 16 and 17 show the "aileron" effect to command aircraft roll accomplished differential deflection of the X-15's horizontal tail "elevon" surfaces. These plots show the change in roll and yaw coefficients as a result of a +/- 1° anti-symmetric deflection of the horizontal tail surfaces. Roll control power is strongest around $M = 1.1$ and declines with increasing Mach Number. The yaw due to roll effect is Mach Number dependent, under certain angle-of-attack and Mach Number combinations, differential "elevon" produces adverse yaw; this occurs when *dCn/dAILERON* has an opposite sign to *dCl/dAILERON*.

As the X-15 attains hypersonic speeds, the increasing dominance of the windward side geometry to vehicle aerodynamics manifests itself in terms of the "quantity" and the "quality" of the aerodynamic roll control power. Flight at hypersonic speeds ($M \sim 6.86$) leads to a factor of four reduction in roll control power compared to flight at $M \sim 1.6$; refer back to FIGURE 16. However, the "quality" of the roll control power improves; we can see that the adverse yaw of the aileron at $\alpha \sim 20^{o}$ is negligible at hypersonic speeds while it is substantial at $M \sim 1.6$.

D. Post Processing the Lateral-Directional Aerodynamic Database

In order to estimate Dutch-Roll lateral directional stability and spin resistance, we need to compute $C_n\beta dynamic$ and the lateral-control-departure-parameter, *LCDP*.

To compute $C_n\beta dynamic$ was must first transform all of the lateral-directional moments into wind axis and then scale $dC_l/d\beta$ by the ratio of rolling moment of inertia to yawing moment of inertia:

$$C_n\beta dynamic = \frac{dC_n}{d\beta} \cdot \cos(\alpha) - \frac{dC_l}{d\beta} \cdot \left(\frac{I_{zz}}{I_{xx}}\right) \cdot \sin(\alpha) \tag{5}$$

For an aircraft to be aerodynamically controllable, it must also have an agreeable Dutch-Roll frequency. Too fast, and the airplane's rigid body mode excites structural resonance. Too slow, and the pilot finds the roll response to be "mushy" with substantial phase-lag that provokes pilot-induced oscillations. MIL STD 8785C [29] supplies a floor of ~0.4-radians/sec for the lateral-directional Dutch-Roll frequency (that is 0.064-Hz or a 15-sec period). When the rigid body frequencies drop below that, the aircraft becomes too unresponsive to pilot with a conventional control strategy. For an exo-atmospheric aircraft like X-15, as the frequencies drop too low the aircraft needs to transition to a reaction control system (RCS) to maintain attitude control.

In order to approximate the Dutch-Roll frequency, we may use a 1-degree-of-freedom simplification where we consider the rigid body aircraft as a pair of lumped masses (defining the mass-moment-of-inertia) and a torsional spring (driven by *Cnβdynamic*). This leads to the simplified Dutch-Roll equation for an inherently stable system:

$$\omega_{dr} \approx \left(\frac{1}{2\pi}\right)\sqrt{\frac{57.4 \cdot C_n\beta\ dynamic \cdot q \cdot S_{ref} \cdot b}{I_{zz}}} \tag{6}$$

In the Dutch-Roll is unstable, we will then use the following equation to estimate the unstable "time-to-double" response:

$$TTD_{dr} \approx \sqrt{\frac{I_{zz}}{-57.4 \cdot C_n\beta\ dynamic \cdot q \cdot S_{ref} \cdot b}} \tag{7}$$

Lastly there is the Lateral Control Departure Parameter – the lateral control departure parameter – if *LCDP* < 0, the adverse yaw from the roll control surfaces overwhelms the static lateral-directional stability of the aircraft precipitating a spin and loss of control. [30] *LCDP* is found using the following equation:

$$LCDP = \frac{dC_n}{d\beta} - \frac{dC_l}{d\beta} \cdot \frac{\left(\frac{dC_n}{d\ aileron}\right)}{\left(\frac{dC_l}{d\ aileron}\right)} \tag{8}$$

Turning next to FIGURE 18, we see that the X-15 baseline aerodynamic database has positive *LCDP* across all flight Mach Numbers over a wide range of angles of attack. This means that the yaw byproducts of aerodynamic roll control, as implemented through differential elevon action on the horizontal tail surface, does not overwhelm the static directional stability of the airframe.

This is encouraging, for if the rigid body frequencies or *LCDP* falls below minimums, we must either avoid the flight regime or transition to a reaction control jet system.

As with longitudinal stability, low frequency conditions will be found "over-the-top" during exo-atmospheric flight where $q \rightarrow 0$ while rigid body modes likely to provoke

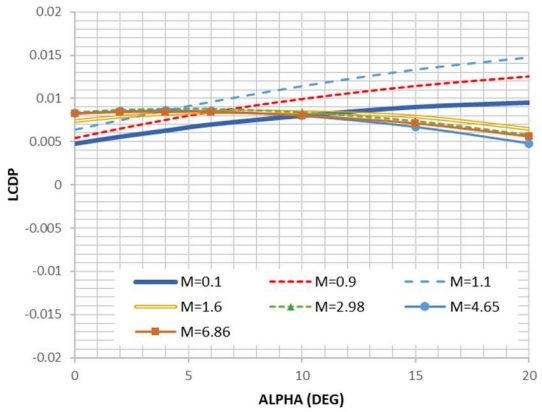

FIGURE 18 – *LCDP* based upon differential elevon ("Aileron") action.

structural resonance will be found during high-speed low altitude flight where *KEAS* >> 1000-knots.

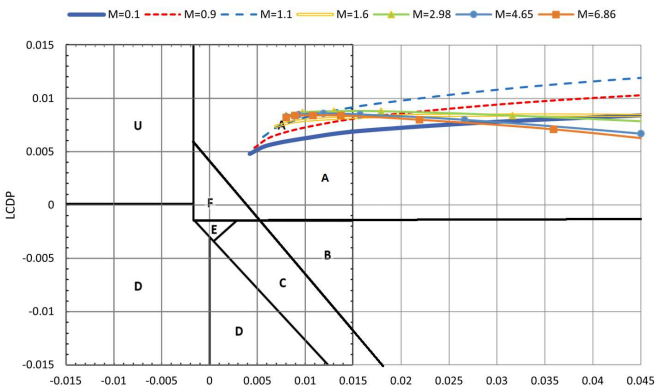

FIGURE 19 – Bihrle-Weissman Chart for the X-15

The inherent airframe resistance to spin is evaluated using the Bihrle-Weissman criteria; see FIGURE 19. [6] Region "A" of a Weissman chart, the region where $C_n\beta dynamic$ and *LCDP* are both positive indicates an airframe inherently resistant to spin. If *Cnβdynamic* and *LCDP* are simultaneously too small, we find ourselves in region "E" or "F" with weak spin and departure resistance. Other unfavorable pairings of *Cnβdynamic* and *LCDP* indicate a propensity to have control induced departure (regions B and C), strong spin tendencies (regions D). If *Cnβdynamic* indicates an unstable Dutch-Roll mode even favorable aileron action (indicated by *LCDP* >> 0) cannot resolve the inherent lack of directional stability.

We can see here, where the full X-15 aerodynamic database has been plotted on the Bihrle-Weissman chart, that the entire speed and angle-of-attack envelope falls into Region "A." Thus, this airframe may be flown at any point in its aerodynamic database without risk of adverse control coupling which could precipitate a spin; in other words, the "quality" of its aerodynamic control effectors do not restrict its flight envelope.

Because the Bihrle-Weissman chart does not assess the "quantity" of roll control power, designers need to consider other metrics to size the roll control surfaces. On less exotic airframes, static lateral-directional trim for a crosswind landing or controlled flight with a critical engine-inoperative (minimum control speed) sizes aileron and rudder. At the present time, we have not developed a high-speed / low-dynamic pressure screening metric to establish minimum lateral-directional control power requirements.

III. Changes to the Point-Mass Mission Simulation

The mission performance tool that is expanded on in this paper was originally coded by Takahashi to simulate typical 14 CFR §25 certified aircraft vehicles flying various missions. [6] Written in VBA, the code inputs three collections of data: an aero performance data, five column performance data, and a mission profile file. It outputs time or distance history plots of a host of useful aerodynamic conditions. Due to its integration with EXCEL the data can be easily exported or further processed.

The five column data does not care whether the engine is air breathing or rocket powered, as such, it does not require an overhaul like the expanded aerodynamic database did. As the name suggests, this file is five columns of data that we used as a lookup table to extract propulsion data for a given engine. It consists of thrust and thrust specific fuel consumption (TSFC) which are subject to the independent variable of flight Mach Number, altitude and power level angle (PLA). With this collection of data, the performance of the propulsion system is fully defined. Data for the X-15's XLR99 engine has been compiled by Maher, et al [32] allowing for simulations of most of the flights but with further work five column data of the initial XLR11 engines could be assembled and then used to simulate the early missions.

The mission profile is a human readable text file that contains the "pilot talk". This talk is a list of commands to be carried out in order. Such typical flights would include commands of climb or descend at constant KIAS or Mach, accelerating, level flight, and ground run up. As well as many state changes such as winds aloft, discrete weight change, adjusting the PLA, and engine failure. New modes are needed as aero-space planes do not climb like standard aircraft, often flying outside of equipoise. Such modes are where the pilot would light the engine and hold a constant angle-of-attack as they climb or a constant coefficient of lift as they reenter.

This non-equipoise flight is solved by summing the four basic forces of lift, drag, weight and thrust in wind axis. First, we find the coefficient of lift, angle-of-attack, flight path angle, thrust, and weight at the previous time step location.

As we are forcing the coefficient of lift or angle-of-attack, we have a closed set of equations and if we then use the five column data to interpolate thrust and the aero database to interpolate the lift or alpha we can have all desired forces. By summing the forces in the horizontal and vertical direction and by plugging them into the classical $F = ma$ equation we can get the acceleration in those directions. Then to find the new velocity of the aircraft we take the previous time step velocity and add the acceleration multiplied by time step size. From these wind axis velocities, we can find the new Mach, change in altitude, and remaining values to get to the next time step.

But given this new non-equipoise flight we must reevaluate the assumptions made during the creation of Takahashi's original code. One such assumption is the small-angle approximation made in order to help simplify the equations of motion. This was perfectly reasonable given that the desired mission simulations would be flying normal commercial operations so the angle-of-attack would not be pushing this approximation. But now that the code is expected to be flying reentry aircraft. We may see vehicles belly flopping their way into the atmosphere. As such, great labor was made to find all such approximations and replace them with appropriate substitutions.

At very high flight speeds, some of the weight of the vehicle may be offset by the centrifugal force resulting from flying at a constant altitude above the spherical earth; where W is flight weight in lbm, V is the true airspeed in ft/sec and the altitude and earth radius are given in ft.

$$LIFTcentrifugal = \frac{W}{32.174}\frac{V^2}{(Alt+EarthRadius)} \tag{9}$$

With these corrections made, the last barrier from high altitude quasi-ballistic simulations is that the mission code was built on a truncated version of the 1962 standard atmosphere valid only to ~100,000-ft. We replaced this model with the far more capable 1976 standard atmosphere [12] which extends up to 282,000 ft providing some "head room" for the X-15 and similar missions.

IV. Analysis

The first simulations we flew with the extended aero database were designed to match the often-depicted mission shown in FIGURE 20. However, upon flying a 5-gee pullout the simulation predicts several atmospheric skips. The only way to reconcile the stated high-gee pullout with the unimodal trajectory is that the X-15 must have been banked over during reentry. This came as a surprise to the authors as no such maneuver is depicted in ConOps diagrams, with the exception of banked maneuvers being meant to align with the runway. However subtle, there is evidence of banked flight for reentry sprinkled in reports. This can be found in the detailed time histories from Holleman [33] and with close inspection of FIGURE 21, showing both vertical and horizontal-gees a_n and a_l, which in that case necessitate up to a 70° bank angle.

We showcase two flights where we have sculpted the mission profile to match their respective time history graphs.

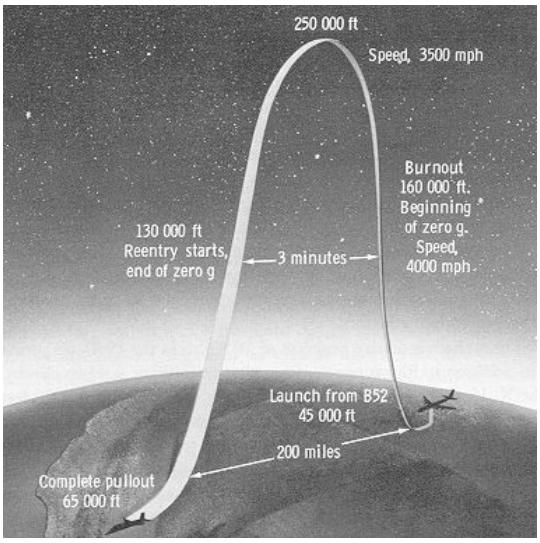

FIGURE 20 – X-15 ConOps

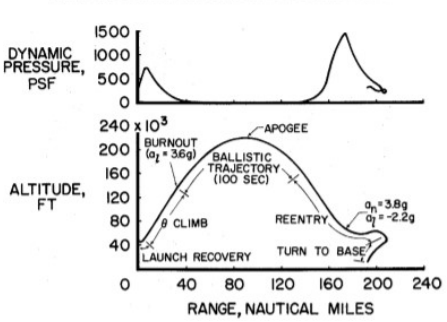

FIGURE 21 – General high-altitude flight from NASA D-1278 [17]

A. EXO-ATMOSPHERIC MISSION

The first flight is the 'HIGH ALTITUDE' case found in NASA TM X-638 [34]; see FIGURE 22. We chose this case for its exo-atmospheric and hypersonic properties. The mission profile is detailed in Table 4 showing the "pilot talk." These stages can be seen in FIGURE 23. Because the NASA trajectory is time stamped $t = 0$ at $M = 1.1$ and $ALT = 47{,}000$-ft, the physical mission starts before our simulation begins.

The result of this profile can be seen plotted on top of the actual data in FIGURE 24 and 25. We see that there is very good agreement between the simulated and actual data.

For most of the flight the angle-of-attack is the controlled variable, FIGURE 26 shows the discrete steps resulting from modes changes over time. From FIGURE 27, we can see that the maximum deflection of the elevator required to trim is 26° which is within the capability of the X-15 showing that it is stable in pitch during the entire flight.

Although the X-15 is always statically stable, refer to FIGURE 28 (overleaf) which shows that ($dC_m/d\alpha < 0$), the stick fixed Short-Period frequency varies widely throughout the mission, refer to FIGURE 29 (overleaf). The stick fixed Short-Period frequency showing that it essentially drops to nothing when "going over the top" of the ballistic trajectory. The sub 1-Hz peaks during high dynamic pressure flight in ascent and descent are not large enough to excite structural resonance for a relatively stiff aircraft like the X-15.

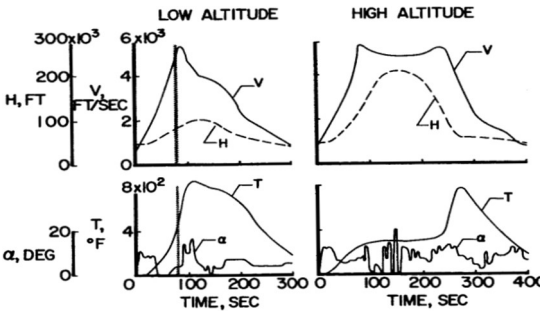

FIGURE 22 – NASA TM X-638 Trajectory [34]

Table 4 Mission Profile NASA TM X-638 (High Altitude)

Segment	Condition
-1→0	$M = 0.8$, $ALT = 45{,}000$-ft, $PLA = 0$, Constant $\alpha = 0°$, drop, ignite motor and begin accel climb
0→1	$M = 1.1$, $ALT = 47{,}000$-ft, $PLA = 1$, Constant $\alpha = 6°$, Until $ALT > 125{,}000$-ft, then cutoff motor
1→2	$PLA = 0$, Constant $\alpha = 6°$, Until $ALT > 200{,}000$-ft
2→3	$PLA = 0$, Constant $\alpha = 5°$, Deploy Brakes, Until $ALT < 160{,}000$-ft
3→4	$PLA = 0$, Constant $\alpha = 16°$, Until $M < 4.5$
4→5	$PLA = 0$, Constant $\alpha = 16°$, Bank 45°, Until $M < 4$
5→6	$PLA = 0$, Constant $\alpha = 14°$, Bank 70°, Until $M < 3.5$
6→7	$PLA = 0$, Constant $\alpha = 12°$, Bank 70°, Until $M < 3$
7→8	$PLA = 0$, Constant $\alpha = 10°$, Bank 60°, Stow Breaks, Until $M < 2$
8→9	$PLA = 0$, Wing Level Decelerate, Until KIAS < 225
9→	$PLA = 0$, Descend at Constant KIAS

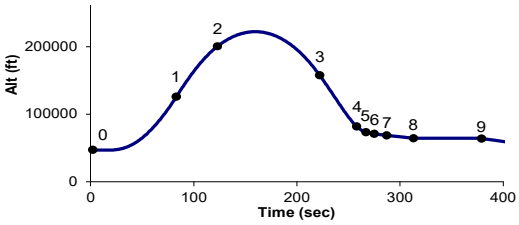

FIGURE 23 – NASA TM X-638 Trajectory

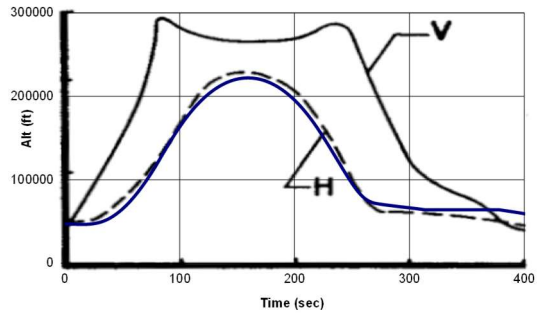

FIGURE 24 – Altitude vs Time

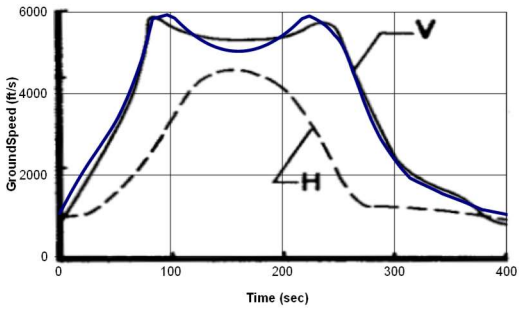

FIGURE 25 – Ground Speed (True Airspeed) vs Time

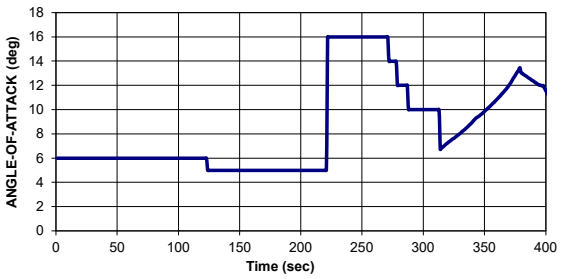

FIGURE 26 – Angle-of-attack vs Time

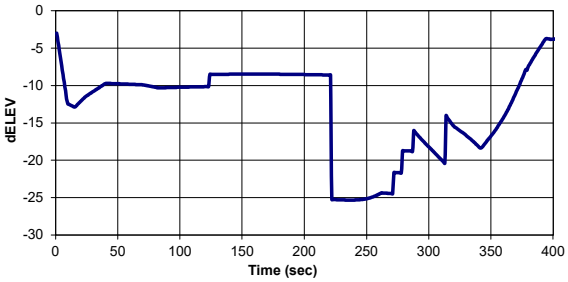

FIGURE 27 – Elevator Deflection vs Time

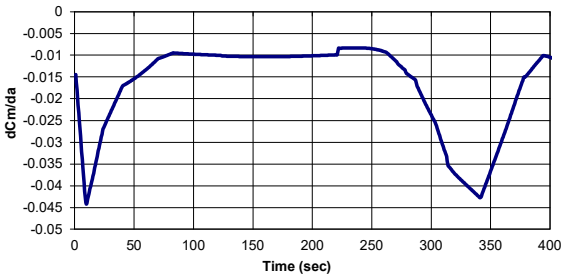

FIGURE 28 – Longitudinal stability vs Time

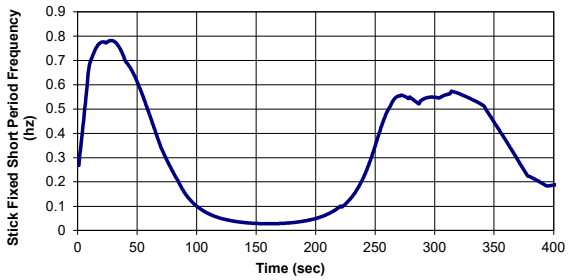

FIGURE 29 – Stick Fixed Short-Period Frequency vs Time

Turning next to look at lateral-directional stability (refer to FIGURES 30 and 31), we can see the same trend that we saw in the longitudinal domain: we see relatively high frequencies during ascent and descent and extremely low frequencies "going over the top". This is not surprising as the dynamic pressure trends towards zero, FIGURE 32, overleaf, even as the flight speed, FIGURE 33, overleaf, peaks at just over $M \sim 5$.

The X-15 will need to rely upon reaction-jet control thrusters for pitch, roll and yaw control augmentation during certain flight phases. Taking into consideration that minimally practical stick-fixed frequencies are ~0.06-Hz longitudinally and ~0.15-Hz lateral-directionally, we can see that X-15 cannot be controlled with satisfactory phase-margin as it flies "over the top" with its aerodynamic surfaces.

Although the rigid-body dynamic response falls below satisfactory limits, the Bhirle-Weissman chart (see FIGURE 34, overleaf) shows very strong spin resistance throughout the entire flight. The X-15 remains firmly in in the 'A' quadrant of the graph from launch, through burnout, over-the-top, reentry, and final glide. This means that the adverse yaw of the roll control aerodynamic surfaces (differential elevon in this case) will never overpower the inherent static directional stability of the X-15. While aerodynamic response will become unresponsive "over the top," the aircraft will continue to respond predictably to roll command inputs.

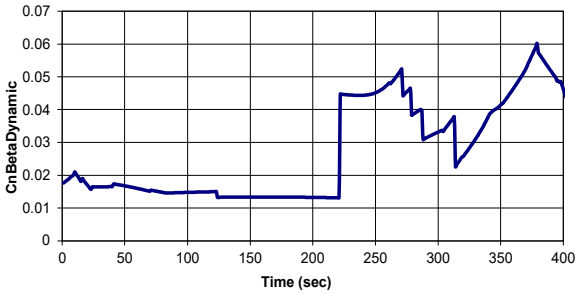

FIGURE 30 – *Cnβdynamic* vs Time

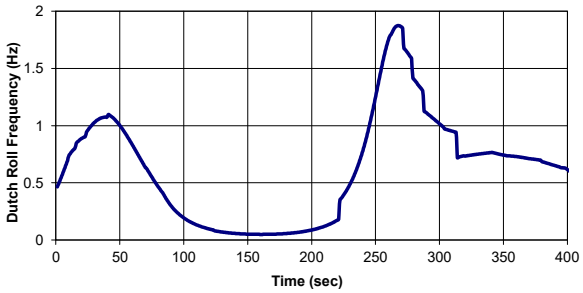

FIGURE 31 – Dutch-Roll Frequency vs Time

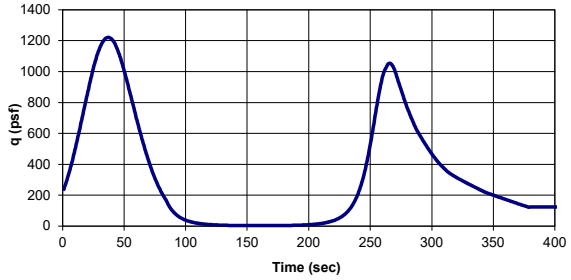

FIGURE 32 – Dynamic Pressure vs Time

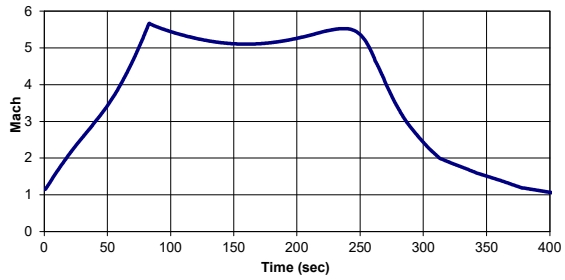

FIGURE 33 – Mach vs Time

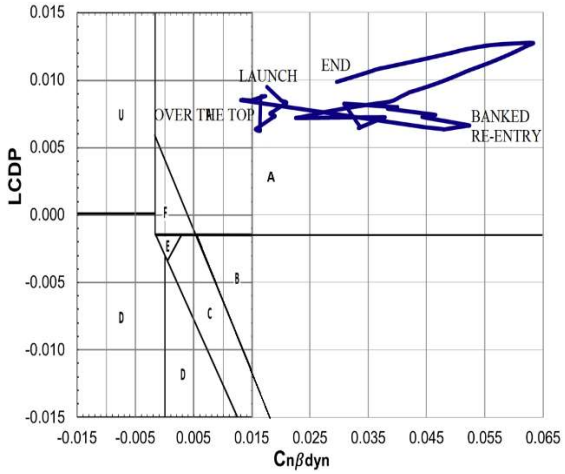

FIGURE 34 – Bihrle-Weissman chart

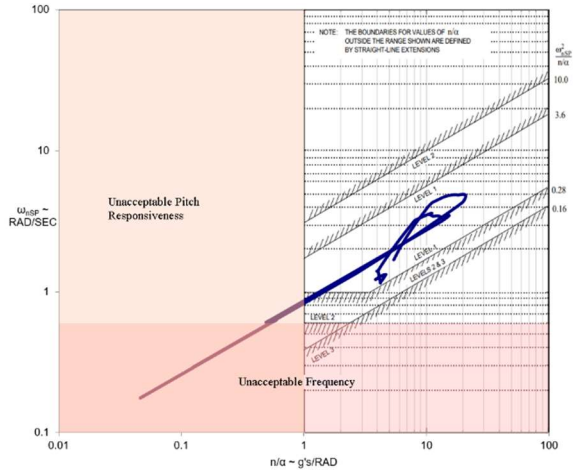

FIGURE 35 – MIL-STD 8785C – Category A

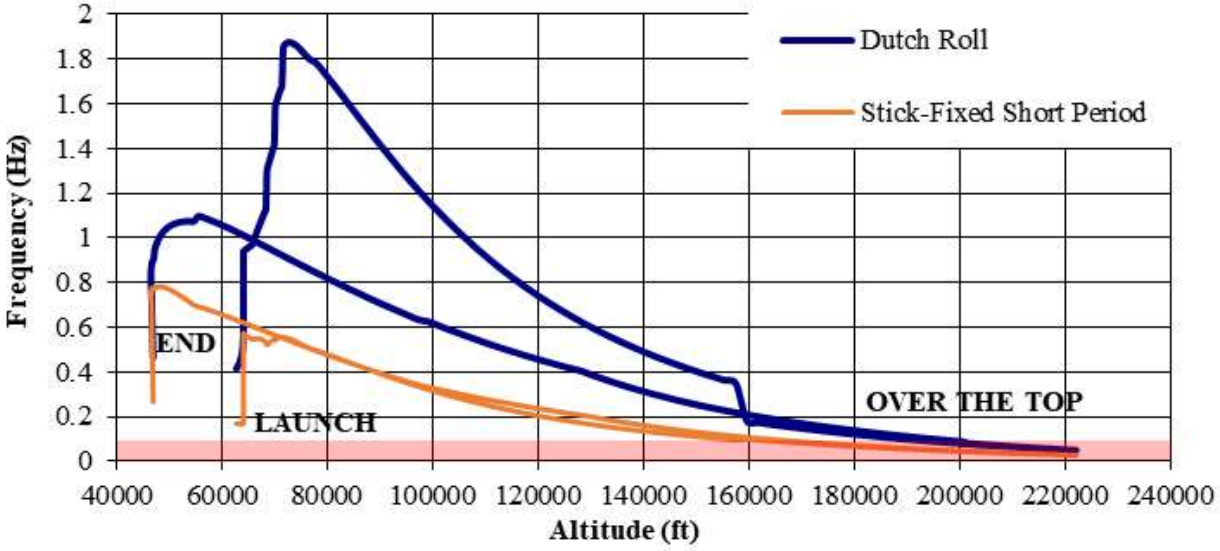

FIGURE 36 – Inertial Coupling Screening - Dutch-Roll and Short-Period vs Altitude

We may further understand why an impulse (as opposed to aerodynamic) control system is needed if we examine the stick-fixed Short-Period frequency in context with pitch responsiveness. Let us revisit the MIL-STD 8785C chart in FIGURE 36. At launch, high-dynamic pressure re-entry and during the final glide, both the Short-Period frequency and pitch responsiveness frequencies are firmly within the *LEVEL 1* zone. But as the X-15 flies "over the top," both the Short-Period and pitch responsiveness both fall to near zero; the flight trace falls "falls off" the left hand side of the chart. As dynamic pressures drop, the X-15 becomes unacceptably poor in pitch responsiveness **and** rigid-body longitudinal frequencies. For this flight, it appears that the pitch responsiveness becomes unacceptable ($n/\alpha < \sim 3$) before the rigid-body frequencies drop below acceptable minimums. In other words, the X-15 has insufficient wing area to "glide" at $nZ=1$ before the longitudinal handling qualities become hopelessly unresponsive.

We may also ask if the X-15 is predisposed to Inertial Coupling. Inertial Coupling exists when the rigid body Dutch-Roll and Short-Period frequencies coincide. When the frequencies align, weakly damped rolling motions may excite pitch oscillations and vice versa. In FIGURE 36, we plot both the Dutch-Roll and Short-Period frequencies as a function of flight altitude. We can see that the frequencies are generally distinct, and only get close to one-another while "going over the top". Since Inertial Coupling is likely to occur only as the X-15 flies "over the top," where the rigid body frequencies are already so low as to need supplemental control from reaction-control, this flight does not raise concern.

B. ENDOATMOSPHERIC HIGH SPEED FLIGHT

We found the second flight documented in NASA TM X-468. [35] We chose to model this as it represents flight within the atmosphere at near hypersonic speeds. The mission profile is detailed in Table 5 with the stages being shown in FIGURE 37.

The result of this profile was plotted on top of the actual data in FIGURE 38-40, overleaf. Once again, we can architect the simulation so that there is very good agreement between the model and flight test data in terms of altitude-vs-time, Mach Number vs time and angle-of-attack vs time.

From FIGURE 41, overleaf, we can see that the maximum deflection of the elevator required to trim is 17°, so no excessive control input is needed to fly this mission.

FIGURE 42, overleaf, plotting $dC_m/d\alpha$ demonstrates that the X-15 is statically stable in pitch during the entire flight.

Due to the lower peak altitude in this flight, the dynamic pressure does not make a near zero dip while "going over the top." FIGURE 43 notes a minimum dynamic pressure of around 200-lbf/ft^2.

The longitudinal stability is good with FIGURE 44 showing the stick fixed Short-Period frequency showing reasonable values throughout the flight. With the lowest frequency (~0.2-Hz) right at the start and never rising above 1-Hz to excite structural resonance.

We can see the same trend with lateral-directional stability. FIGURE 45 shows a positive *Cnβdynamic* throughout the flight. The stick-fixed Dutch-Roll frequencies, see FIGURE 46, also seem reasonable with the lowest frequencies seen during launch and the highest frequencies peaking at just over 1-Hz during the Mach 3 / 75,000-ft pull-up up maneuver around t = 280-sec.

We revisit the Bihrle-Weissman chart in FIGURE 48 and see that the X-15 once again shows very strong spin resistance throughout the flight. It remains firmly in in the 'A' quadrant of the graph from launch, through burnout, the Mach 3 / 75,000-ft pull-up maneuver, as well as descent and approach.

For this flight, the X-15 does not need any sort of assistance from reaction control jets. Examine the MIL-STD 8785C chart for this mission in FIGURE 48. Both the Short-Period frequency and pitch responsiveness frequencies are firmly within the *LEVEL 1* zone at all times.

Table 5 Mission Profile

Segment	Condition
0→1	M = 0.8, ALT = 45000-ft, PLA = 0, Constant α = 0°, Until t = 12-sec
1→2	PLA = 0.5, Constant α = 11°, Until t = 40-sec
2→3	PLA = 1, Constant α = 9°, Until t = 60-sec
3→4	PLA = 1, Constant α = 8°, Until t = 240-sec
4→5	PLA = 1, Constant α = 2°, Until t = 285-sec, then cutoff motor
5→6	PLA = 0, Constant α = 8°, Until t = 295-sec
6→7	PLA = 0, Constant α = 4°, Until t = 305-sec
7→8	PLA = 0, Level Decelerate Until M < 1.8
8→	PLA = 0, Descend at constant KIAS

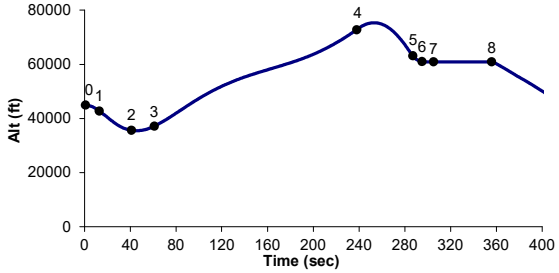

FIGURE 37 – NASA TM X-468 Trajectory

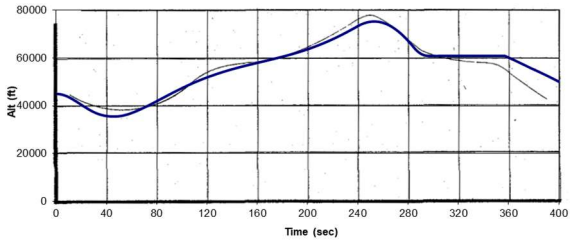

FIGURE 38 – Altitude vs Time

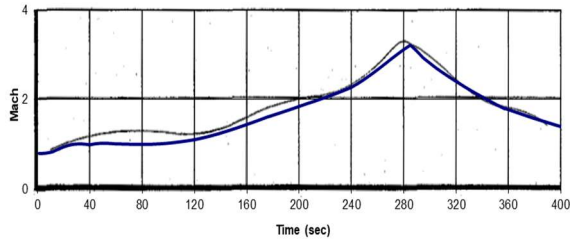

FIGURE 39 – Mach vs Time

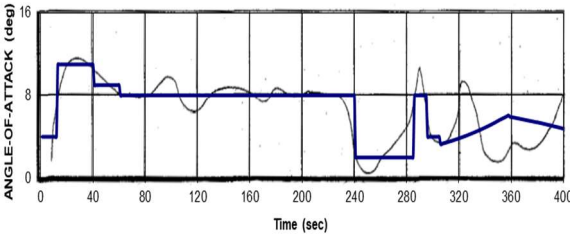

FIGURE 40 – Angle-of-attack vs Time

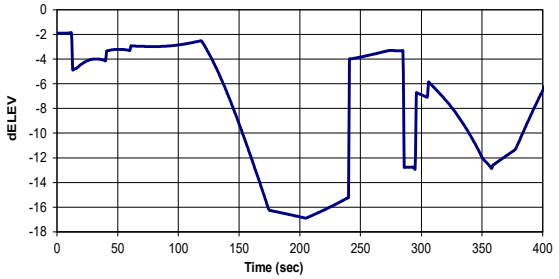

FIGURE 41 – Elevator Deflection vs Time

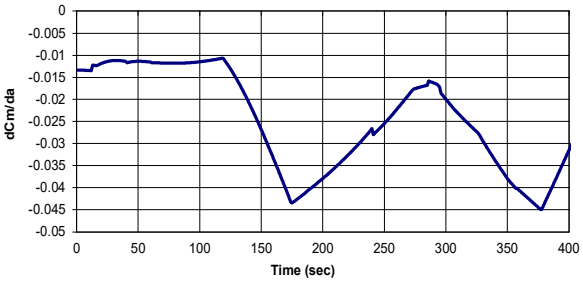

FIGURE 42 – Pitch Stability vs Time

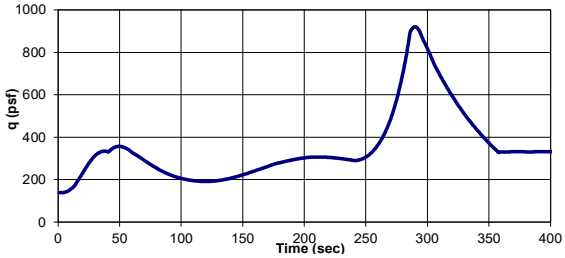

FIGURE 43 – Dynamic Pressure vs Time

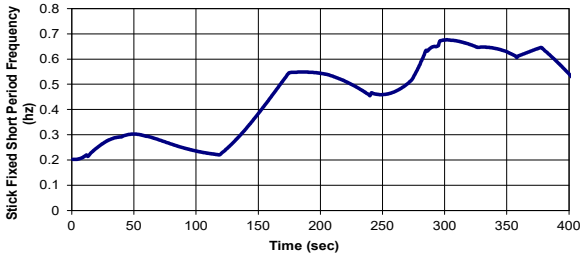

FIGURE 44 – Stick Fixed Short-Period Frequency vs Time

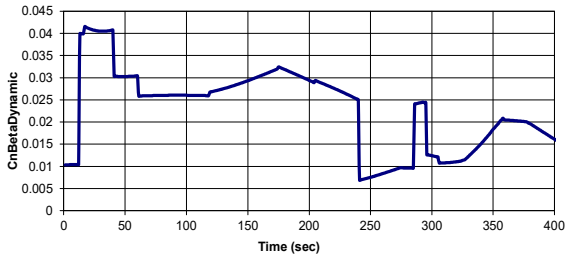

FIGURE 45 – CnβDyanmic vs Time

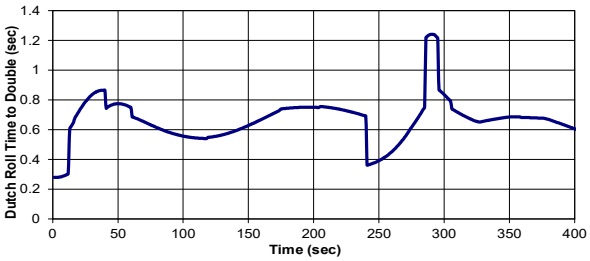

FIGURE 46 – Dutch-Roll Frequency vs Time

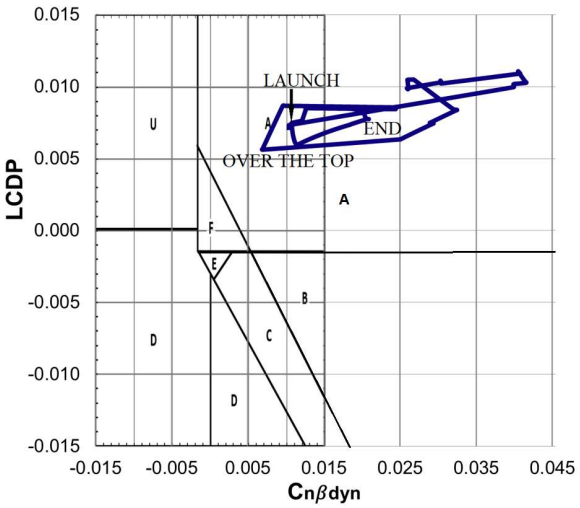

FIGURE 47 – Bihrle-Weissman chart

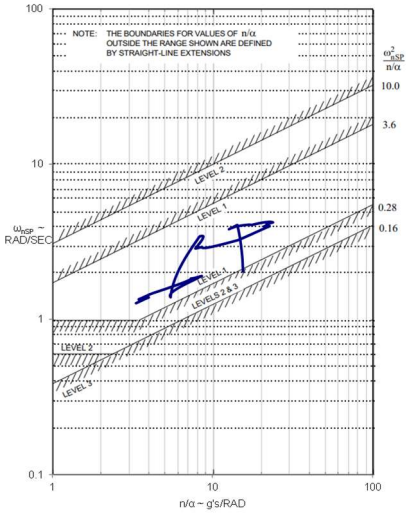

FIGURE 48 – MIL-STD 8785C – Category A

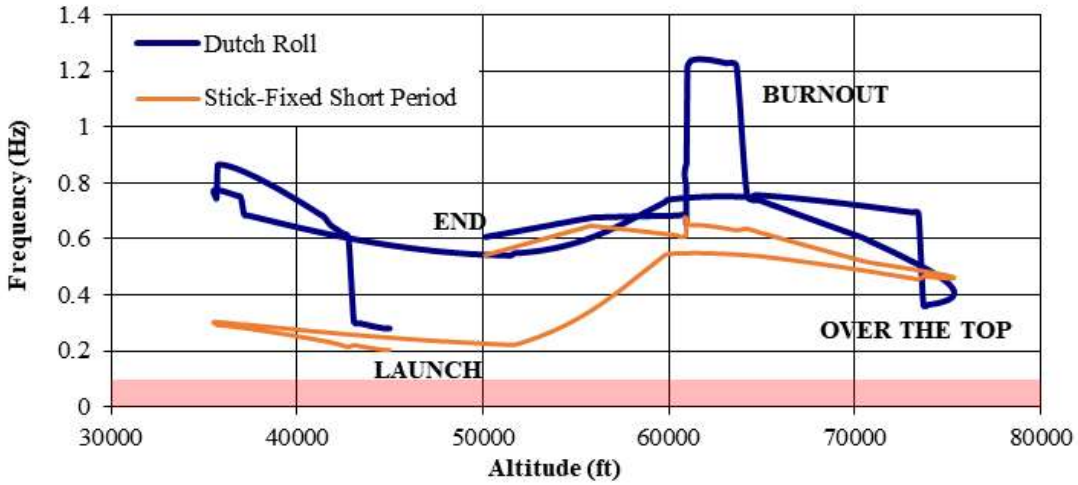

FIGURE 49 – Inertial Coupling Screening - Dutch-Roll and Short-Period vs Altitude

For this flight, we may also ask if the X-15 is predisposed to Inertial Coupling. Recall, on the exo-atmospheric flight we predict a tendency for Inertial Coupling "over the top" where it would not be dangerous. In FIGURE 49, where we plot both the Dutch-Roll and Short-Period frequencies as a function of flight altitude, we can see that the frequencies are generally distinct but do cross twice as the X-15 flies "over the top" at ~75,000-ft at ~0.45-Hz. The frequencies are rather close through much of the gliding descent below 60,000-ft with both frequencies predicted ~0.6-Hz. Since this portion of the mission is flown at high-dynamic pressure, this is the potential for considerable energy crosstalk between these modes.

V. Discussion

Between our estimation of the inherent aerodynamics and our reconstruction of several published flights, we see that the X-15 was designed to be a very controllable aircraft. The most obvious stability problem arises from its rigid-body modes.

For the high altitude mission, where the X-15 essentially leaves the atmosphere so regardless of its speed the dynamic pressure falls to zero. As such, the frequencies and aerodynamic pitch responsiveness also fall towards zero. With unacceptable aerodynamic control in a near vacuum, the aircraft must employ control methods such as a reaction control impulse jet system. The good news for the X-15 was that it did not suffer from any sort of control coupling (Weissman Chart) tendency to incite a spin. Thus, it was easy to devise a blended strategy for the pilot to transition from aerodynamic to impulse thruster control; see FIGURE 50.

Our analysis of the Mach 3, lower altitude flight showed acceptable magnitude for the rigid-body frequencies. However, we noted that the mass properties of the X-15 led to a situation where the rigid body Short-Period and Dutch-Roll modes were very similar over a significant portion of the flight (especially the peak-altitude hypersonic "cruise" point). This detailed flight control system would need to carefully consider how to damp both the Short-Period and the Dutch-Roll mode in light of similar (~0.5-Hz or ~2-second period) oscillations.

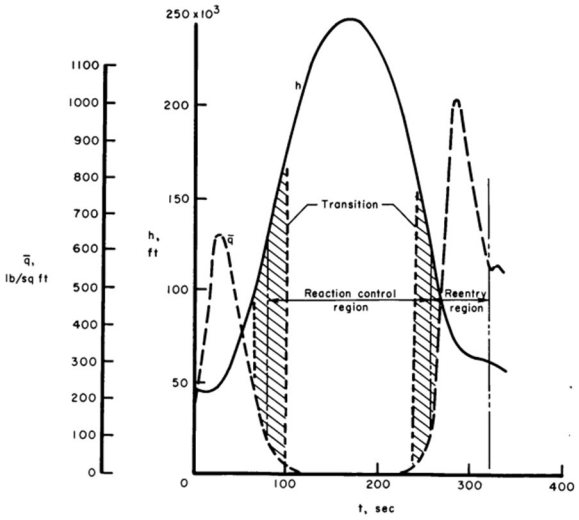

FIGURE 50 – Reaction control region for X-15 different but typical high altitude flight after TN 2864 [36]

Unlike the X-15, the Space Shuttle Orbiter configuration did not achieve favorable inherent lateral-directional stability and controllability during its high speed flight. While *Cnβdynamic* was positive from de-orbit (Mach 25) through re-entry all the way to the ground, *LCDP* became unfavorable above approximately $M = 1.5$. Similar to the X-15, the Orbiter's rudder was ineffective at high speeds (above Mach 3) and high angles of attack. Unlike the X-15, which had favorable *LCDP* throughout its entire flight envelope, the Orbiter has a major problem because no combination of "aileron-rudder-interconnect" can resolve its inherent spin tendency arising from aerodynamic roll commands. Thus, the Space Shuttle Orbiter used its active "yaw control" reaction control system not only during low dynamic pressure flight, but all the way down to $M = 1$ at altitudes < 50,000-ft altitude. According to a USAF report, the shuttle fielded control laws and gains which automatically blended aileron, rudder and reaction-control jets from $M = 3$ down to $M = 0.9$. On mission STS-9, flight test data revealed a need to augment aerodynamic control with the reaction-control jets deep into the transonic. Modifications to the control laws, implemented on STS-13 reduced RCS propellant usage but did not eliminate the need for reaction-control-jets above $M = 1.6$. [37]

VI. Conclusions

In this paper, we developed an aerodynamic database for the North American X-15 along with a general purpose kinematic simulation that could closely match the trajectory of the actual aircraft as it was flown on several missions. The handling qualities screening parameters that we track: Short-Period frequency, Dutch-Roll frequency, elevator to trim, *Cnβdynamic* and *LCDP* confirm a stable and controllable aircraft under atmospheric flight conditions. We will further show that our screening parameters: 8785C longitudinal pitch responsiveness vs Short-Period Frequency and Minimum Stick Fixed Dutch-Roll frequency anticipate the transition to Reaction Control as the aircraft leaves the atmosphere. The screening approach implemented here will be useful to support design trades for future hypersonic vehicles. These same screening parameters will be able to identify deficiencies in tail and control surface sizes and suggest regions of the flight where a RCS system will be needed to augment aerodynamic control whether due to low dynamic pressure or to mitigate against unfavorable control coupling.

Acknowledgements

This research was supported in part by an appointment to the Postgraduate Research Participation Program at the U.S. Air Force Institute of Technology, administered by the Oak Ridge Institute for Science and Education through an interagency agreement between the U.S. Department of Energy and AFIT.

References

[1] Gorman, S. "Billionaire Branson soars to space aboard Virgin Galactic flight," Reuters, July 12, 2021. https://www.reuters.com/lifestyle/science/virgin-galactics-branson-ready-space-launch-aboard-rocket-plane-2021-07-11/

[2] Anon., "Russia says it successfully tested hypersonic missile praised by Putin," Reuters, July 19, 2021. https://www.reuters.com/world/europe/russia-conducts-ship-based-hypersonic-missile-test-ifax-cites-defence-ministry-2021-07-19/

[3] Stone, M., "U.S. successfully flight tests Raytheon hypersonic weapon – Pentagon," Reuters, September 27, 2021. https://www.reuters.com/world/us/us-successfully-flight-tests-raytheon-hypersonic-weapon-pentagon-2021-09-27/

[4] *Jet Transport Performance Meth*ods, Boeing Flight Operations Engineering Training Document D6-1420, 7th Edition, Boeing, Seattle, WA, May 1989

[5] Takahashi, T.T., *Aircraft Performance and Sizing, Volume I: Fundamentals of Aircraft Performance*, Momentum Press, New York, 2016.

[6] Takahashi, T.T., *Aircraft Performance and Sizing, Volume II: Applied Aerodynamic Design*, Momentum Press, New York, 2016.

[7] Hargraves, C. R., and Paris, S. W., "Direct Trajectory Optimization Using Nonlinear Programming and Collocation ," AIAA Journal of Guidance, Control, and Dynamics, Vol. 10, No. 4, 1987, pp. 338-342.

[8] Brauer, G.L., Cornick, D.E. and Stevenson, R. "Capabilities and Applications of the Program to Optimize Simulated Trajectories (POST)," NASA CR-2770, Feb 1977

[9] Kauffman, H.G., Grandhi, R.V., Hankey, W.L., Belcher, P.J, "Improved Air Breathing Launch Vehicle Performance with the Use of Rocket Propulsion," J. Spacecraft & Rockets, Vol. 28, No. 2, 1991, p. 172-178.
[10] Kauffman, H.G., Grandhi, R.V., Hankey, W.L., Belcher, P.J, "Optimum Design of Transitions in Climb/Cruise/Descent for Hypersonic Cruise Vehicles," Eng. Opt., Vol 19, 1992, pp. 153-170.
[11] North American Aviation, "USAF Series X-15 Aircraft Interim Flight Manual," 18 March 1960.
[12] Anon. "U.S. Standard Atmosphere, 1976," NASA-TM-X-74335, October 1976.
[13] Anon. "Proceedings of the X-15 First Flight 30th Anniversary Celebration." NASA CP-3105, 1989.
[14] Jenkins, D.R. and Landis, T.R., Hypersonic: The Story of the North American X-15, Specialty Press, North Branch, MN, 2003.
[15] Anon., "X-15 Research at the Edge of Space," NASA EP-9, 1964.
[16] Miranda, L.R., Baker, R.D., and Elliot, W.M., "A Generalized Vortex Lattice Method for Subsonic and Supersonic Flow", NASA CR 2875, 1977.
[17] Weill, J. "Review of the X-15 Program," NASA TN D-1278, 1962.
[18] Walker, H.J. and Wolowicz, C.H. "Stability and Control Derivative Characteristics of the X-15 Airplane," NASA TM-X-714, 1962.
[19] White, R.M., "Resume of Handling Qualities of the X-15 Airplane," NASA TM X-715, 1962.
[20] Franklin, A.E., and Lust, R.M., "Investigation of the Aerodynamic Characteristics of a 0.067-Scale Model of the X-15 Airplane (Configuration 3) at Mach Numbers of 2.29, 2.98, and 4.65," NASA TM-X-38, 1958.
[21] Osborne, Robert S., "Stability and Control Characteristics of a 0.0667-scale Model of the Final Version of the North American X-15 Research Airplane (Configuration 3) at Transonic Speeds," NASA TM X-738, 1962.
[22] Penland, Jim A.; and Fetterman, David E., Jr.: Static Longitudinal, Directional, and Lateral Stability and Control Data at a Mach Number of 6.83 of the Final Configuration of the X-15 Research Airplane. NASA TM X-236, 1960.
[23] Walker, H.J. and Wolowicz, C.H. "Theoretical Stability Derivatives for the X-15 Research Airplane at Supersonic and Hypersonic Speeds Including a Comparison with Wind Tunnel Results," NASA TM X-287, 1962.
[24] Penland, J.A., Ridyard, H.W. and Fetterman, D.E., Jr. "Lift, Drag and Static Longitudinal Stability Data from an Exploratory Investigation at a Mach Number of 6.86 of an Airplane Configuration having a Wing of Trapezoidal Planform," NACA RM 54L03b, 1955.
[25] Souders, T.J. and Takahashi, T.T., "VORLAX 2020: Making a Potential Flow Solver Great Again," AIAA 2021-2458, 2021.
[26] Feagin, R. C., and Morrison,W. D., "Delta Method, An Empirical Drag Buildup Technique," Lockheed-California Co., Rept. LR-27975-VOL-1, 1978.
[27] Saltzman, E.J. and Garringer, D.J. "Summary of Full-Scale Lift and Drag Characteristics of the X-15 Airplane," NASA TN D-3343, March 1966.
[28] Saltzman, E.J., "Preliminary Full-Scale Power-Off Drag of the X-15 Airplane for Mach Numbers from 0.7 to 3.1," NASA TM-X-430, 1960.
[29] Anon., "Flying Qualities of Piloted Airplanes," MIL STD-8785C, U.S. Department of Defense, Washington, D.C., November 5,1980.
[30] Day, R.E. "Coupling Dynamics in Aircraft Design: A Historical Perspective," NASA SP-532, NASA, 1997.
[31] Petersen, F.S., Rediess, H.A and Weil, J., "Lateral-Directional Control Characteristics Of The X-15 Airplane", NASA TM X-726, NASA, 1962.
[32] Maher, J.F, Ottinger, C.W., and Capasso, V.N., "YLR99RM-1 Rocket Engine Operating Experience in the X-15 Aircraft," NASA TN-D-2391, July 1964.
[33] Holleman, E.C. "Summary of High-Altitude and Entry Flight Control Experience with the X-15 Airplane", NASA TN D-3386, April 1966.
[34] Banner, R.D., Kuhl, A.E. and Quinn, R.D. "Preliminary Results of Aerodynamic Heating Studies on the X-15 Airplane," NASA TM X-638, 1962.
[35] Reed, R.D., and Watts J.D., "Skin and Structural Temperatures Measured on the X-15 Airplane During a Flight to a Mach Number of 3.3." NASA TM-X-468, 1961.
[36] Jarvis, C.R. and Lock, W.P. "Operational Experience With The X-15 Reaction Control And Reaction Augmentation Systems" NASA TN D-2864, 1965.
[37] Anon. "Flight Test Results from the Entry and Landing of the Space Shuttle Orbiter for the First Twelve Orbital Flights," AFFTC-TR-85-11, United States Air Force – Flight Test Center, June 1985.